ROYAL SOCIETY OF CHEMISTRY

PAPER

Check for updates

Manipulating the triboelectric surface charge density of polymers by low-energy helium ion irradiation/implantation†

Shuyao Li, ‡[abc] Yong Fan, ‡[b] Huaqiang Chen,[b] Jinhui Nie,[ac] Yanxia Liang,[b] Xinglin Tao,[ac] Jian Zhang,[d] Xiangyu Chen, *[ac] Engang Fu *[b] and Zhong Lin Wang *[ace]

Triboelectric materials and their modification methods are the cornerstones for fabricating triboelectric nanogenerators (TENGs). Numerous modification methods have been proposed for TENGs, while a highly effective and long-term stable method is still under exploration. Here, a surface modification method using low-energy ion irradiation has been proposed for tuning the chemical structures and functional groups of triboelectric polymers at the molecular level. The low-energy ion irradiation brings negligible change to the surface roughness at the micro-scale and mechanical flexibility of the target polymer, while it can provide a stable modification of the electrification performance. Systematic studies about the chemical structure changes in four different polymers induced by ion irradiation can bring insight into the interaction between different chemical groups and electrification performance. A Kapton film modified by ion irradiation shows several unprecedented characteristics, such as high surface charge density, excellent stability and ultrahigh electron-donating capability, and not only creates a new record in the tribo series, but also provides a good demonstration for regulating electrification behavior based on controllable chemical structure change. This study can open up a series of possible breakthroughs in the production of triboelectric materials with diversified properties, which can promote the study of TENGs from a very fundamental level.

Broader context

With the fast development of the internet of things, a large number of sensors and microelectronic devices are applied for supporting this huge information network. Accordingly, this requires the united strength of both batteries and energy harvesting techniques to power all these mobile devices. Ever since 2012, triboelectric nanogenerators (TENGs) have gradually become the mainstream technique in the field of energy harvesting, due to their universal applicability, low cost and high efficiency. Triboelectric materials are the core elements for the fabrication of TENGs, while a highly effective and long-term stable modification method for triboelectric materials is still under exploration. In this study, based on a high-fluence ion irradiation technique, a different modification method has been proposed to directly manipulate the chemical bonds and functional groups of triboelectric polymers at the molecular level, which can change the polymer's 'gene' for contact electrification. A triboelectric film modified by this method shows several unprecedented characteristics, such as ultrahigh electron-donating capability and excellent stability, and creates a new record in the tribo series. A variety of possible breakthroughs in the production of triboelectric materials with diversified properties can be expected based on the results of this study.

[a] CAS Center for Excellence in Nanoscience, Beijing Key Laboratory of Micro-nano Energy and Sensor, Beijing Institute of Nanoenergy and Nanosystems, Chinese Academy of Sciences, Beijing 100083, P. R. China. E-mail: chenxiangyu@binn.cas.cn

[b] State Key Laboratory of Nuclear Physics and Technology, Department of Technical Physics, School of Physics, Peking University, Beijing 100871, P. R. China. E-mail: efu@pku.edu.cn

[c] School of Nanoscience and Technology, University of Chinese Academy of Sciences, Beijing 100049, P. R. China

[d] College of Energy, Xiamen University, Xiamen, 36100, P. R. China

[e] School of Materials Science and Engineering, Georgia Institute of Technology, Atlanta, GA 30332-0245, USA. E-mail: zhong.wang@mse.gatech.edu

† Electronic supplementary information (ESI) available. See DOI: 10.1039/c9ee03307f

‡ These authors contributed equally.

Introduction

Triboelectric nanogenerators (TENGs), as highly efficient and low-cost energy harvesting devices, have been intensively investigated in recent years.[1–6] Compared to other energy harvesting devices, TENGs have several important breakthroughs, including their capability of scale up, their flexible structure design and the unlimited choices of materials, all of which make TENGs one of the mainstream technologies of new energy devices.[7–11] Material selection is the first step in the fabrication of TENGs, since two materials with very different electron affinities can provide a large amount of charge transfer.[10–16]

In addition to the choice of materials, there are several surface modification methods to further elevate the tribo-induced charge density, such as the modification of surface morphologies,[15,16] chemical coating[17–19] and charge/ion injection.[20,21] The inductively coupled plasma (ICP) etching technique is a commonly employed method to design micro-nano structures or patterns on the surfaces of triboelectric materials. Although the major contribution of these micro-nano structures is to increase the effective contact area, the enhancement of triboelectric charge in the micro-nano structures has a low upper limit. Chemical methods can be used to attach different functional groups to the surfaces of polymers, which can not only elevate their charge density but also change their polarity during the contact electrification.[22,23] Nevertheless, chemical modification methods are usually complex, costly, environmentally unfriendly, and their output stability are usually weaker than that of ICP etching. Corona polarization is also an efficient method for amplifying tribo-charge density, which can directly inject electrostatic charge onto the surfaces of dielectric materials. As reported by Wang et al.,[24] the saturated surface charge density through corona polarization can reach 240 μC m^{-2}, which is several times higher than its original value. However, this method is only for polarizable materials and its high performance is also jeopardized by the charge relaxation phenomenon after polarization. Thus, it is still necessary to explore different surface modification methods, in order to further boost the performance of TENGs.

On the other hand, ion irradiation is a widely used research method in many fields such as metal materials, superconducting materials, semiconductor materials, and catalytic materials nowadays.[25–29] Because of its controllable irradiation area, adjustable irradiation dose and uniform irradiation results, it attracts attention in surface physics. It mainly changes the crystal structures of materials through nuclear energy loss and electron energy loss, introduces defects and promotes the formation and quenching of nanocrystals, which can all be used to change the properties of the materials. The effect of ion irradiation on organic materials, especially high molecular weight polymer materials, has attracted increasing attention.[27,28] Elastic and inelastic collisions produced by ion irradiation cause macromolecules in polymers to reach a chemical bond energy barrier and finally break. A lot of free radicals, which can be generated by the breaking of the old bond, combine with ions, and new chemical bonds are formed due to the rearrangement of the structure. The irradiation-induced changes in the mechanical properties of polymers have been thoroughly studied by previous researchers, including their strength, toughness, embrittlement, surface roughness and optical properties.[29] However, the irradiation-induced changes in the electrification performance of polymers have never been considered before. The radiation-induced free radicals and the chemical bonds can increase the surface states for contact electrification and the electron binding energy of the polymer molecule may also be changed due to the generation of new functional groups, all of which indicate a new application direction for the traditional ion irradiation technique.

In this paper, a surface modification method based on low-energy ion irradiation has been proposed to directly manipulate the chemical bonds and functional groups of triboelectric polymers at the molecular level. The low-energy ion irradiation brings negligible change to the surface roughness and mechanical flexibility of the target polymer, while it can provide a stable modification of its electrification performance. Systematic studies about the chemical structure changes in four different polymers induced by ion irradiation have been provided, including the measurements of Attenuated Total Reflectance Fourier Transform Infrared (ATR-FTIR) spectra, molecular dynamics simulation and so on, which help us to better understand the electrification process at the molecular level. A Kapton film modified by ion irradiation shows several unprecedented characteristics, such as high surface charge density (332 μC m^{-2}), excellent stability (>60 days) and ultrahigh electron-donating capability, which allows it to lose electrons during the contact with almost all the previously reported triboelectric materials, such as Nylon, carbon flakes, and food-grade oil-resistant Buna-N rubber. High quality triboelectric polymers are the cornerstone of TENG devices, and this study opens up a different approach to modify the characteristics of triboelectric polymers. A series of possible breakthroughs in the production of triboelectric materials with diversified properties can be expected based on the results of this study.

Results

The experimental process of ion irradiation and the set-up for the irradiation system are shown in Fig. 1a. In order to protect the target polymer from crystallization and carbonization during the irradiation process, a low-energy ion beam of 50 keV is used to irradiate the target sample. During the contact electrification, the surface region with a depth of tens of nanometers plays an important role in charge transfer and the ions irradiated with this low-energy can precisely modify the material in this thickness region. Four kinds of polymers (Kapton $(C_{22}H_{10}O_5N_2)_n$, PET $(C_{10}H_8O_4)_n$, PTFE $(CF_2–CF_2)_n$, and FEP $(C_5F_{10}H_2)_n$), which are common electrification materials for TENGs, are selected as the target polymers for ion irradiation. The He ion is chosen as the implantation ion due to its high electronegativity and stability. The Monte Carlo (MC) method, which is a well-established computer simulation method, has been employed to analyze the transport and penetration processes
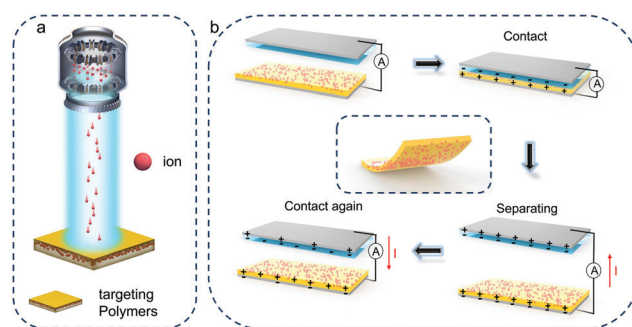

Fig. 1 (a) Schematic diagram of ion irradiation simulation. (b) Schematic diagram of a TENG electrification process.

of particles in polymer materials.[30] This computer simulation can track the transport and collision of a large number of incident particles in the medium, the energy loss and various parameters of the secondary particles can be calculated throughout the irradiation process by the stopping and range of ions in matter (SRIM). The ions are incident on the surface of the material, and their trajectory in the solid is not a straight line but a broken line. The path through which ions actually travel in a solid is called the total range, which is expressed as R. R_P is defined as the projection of the total range R of the ions in the direction of their incident velocity. The total range R of ions in the solid can be expressed as:

$$R = \int_0^{E_0} \frac{dE}{-dE/dx} = \int_0^{E_0} \frac{dE}{NS(E)} \qquad (1)$$

where E_0 is the initial energy, $(-dE/dx)$ is the stopping power to describe the energy loss per unit length of the energetic ions in the solid, N is the atomic number density of the target and $S(E)$ is the tissue cross section related to the stopping power of each target atom. Then, the movement process of the ions and the concentration distribution of the ions in the solid are obtained based on the ion collision free path λ, the scattering angle θ_r in the experimental coordinate system, the azimuth angle X of the velocity and other physical parameters. Finally, by keeping the R_P constant, we can design different irradiation experiments, and the depth profiles of the atomic displacement damage and ion concentration from the SRIM estimation are given in Fig. S1a and b (ESI†). Three damage levels at the peaks are 0.026, 0.26, and 2.6 dPa, and three concentrations of He are

also achieved. The irradiated polymers are made into contact–separation mode TENGs to study their electrification performance, and the working mechanism of the contact–separation mode TENG is based on the combined effects of contact electrification and electrostatic induction, as shown in Fig. 1b. For the contact–separation mode TENG, the contact of two tribo materials leads to charge generation on the contact interface and the transfer of electrons from the surface states of one dielectric to those of the other is the dominant process for this charge generation.[31] When separated, the tribo-charges with opposite polarities are left on the surfaces of dielectrics and the established electrostatic field between them can induce displacement current in the external circuit. By checking the transferred charges and established electrostatic field from the TENG devices, we can decide the generated surface charge density on the triboelectric polymers and the performance change of the triboelectric polymers induced by ion irradiation can be revealed accordingly.

The electrification performances of the different ion-irradiated polymers are systematically studied and the results are summarized in Fig. 2. Firstly, the ion dose of irradiation applied to four polymers is fixed at 1×10^{16} ions per cm^2 (see Fig. 2a–d), and the performance changes of the four polymers before and after irradiation are measured, respectively. In this experiment, the irradiated polymers are selected as the first tribo materials, while the second tribo material is always Al foil, as can be seen in Fig. 2e–h. The effective contact areas for the TENG devices in Fig. 2 are all kept at 7 mm × 7 mm. The irradiated Kapton film shows the most significant performance change during the contact electrification. As shown in Fig. 2e, the output voltage
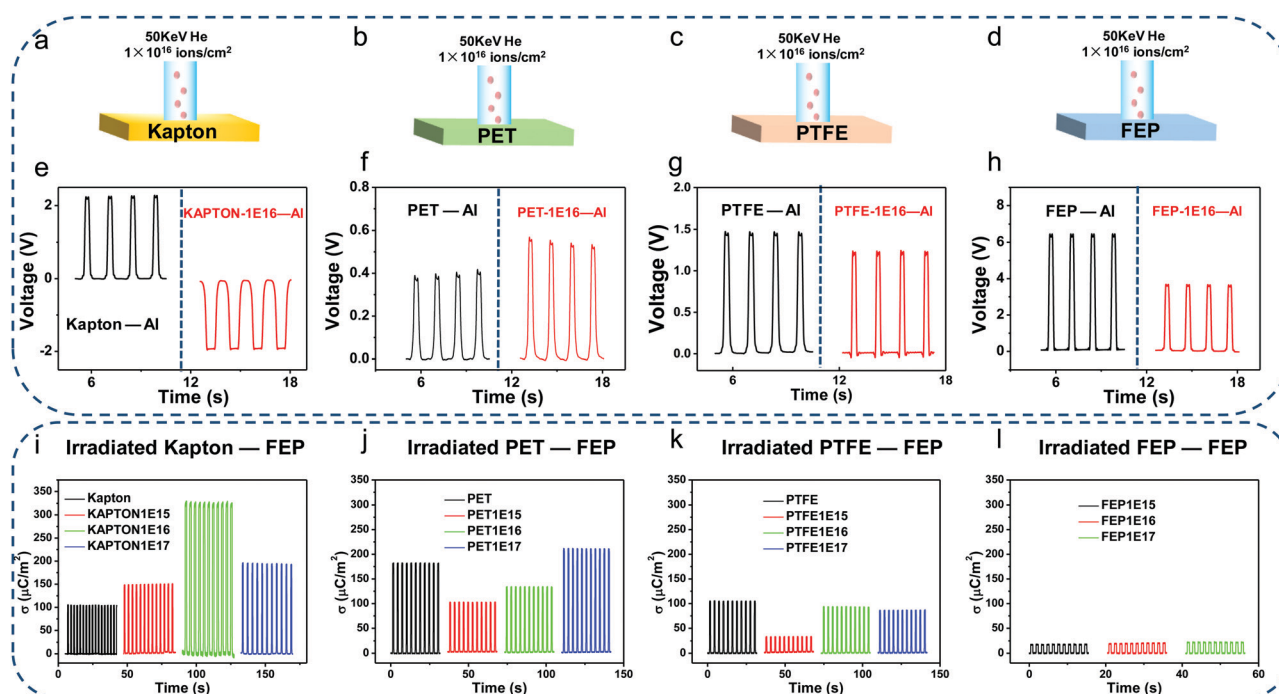
Fig. 2 (a–d) Schematic diagrams of four polymers irradiated with 1×10^{16} He ions per cm^2. The effective contact areas for the TENG devices are all kept to be 7 mm × 7 mm. The contact–separation type TENG devices are employed for the measurements and the output voltages of the pre-irradiation and post-irradiation polymers contacting with Al foil: (e) Kapton, (f) PET, (g) PTFE, and (h) FEP. Maximum transferred charge densities (σ) of different kinds of irradiated polymers contacting with FEP: (i) Kapton, (j) PET, (k) PTFE, and (l) FEP.

from the TENG device changes its polarity (from 2.2 V to -2 V) after the irradiation treatment is applied to the Kapton film, which means that the Kapton film changes from an electron-accepting material to an electron-donating material due to He-irradiation. The output voltages from the other three devices (PET-Al, PTFE-Al and FEP-Al) only show slight differences and the polarities of the polymers also remain unchanged, as can be seen in Fig. 2f–h. It is interesting to find that the electrification performance of the irradiated FEP is suppressed, while the output voltage from the irradiated PET is increased in comparison with its original results (Fig. 2f and h), suggesting that the same ion irradiation can induce different performance changes for the different polymers.

The Al foil in the current experiment is a common positive type triboelectric material and it is also necessary to study the interaction between irradiated polymers and negative triboelectric materials. The FEP film is a typical negative triboelectric material that has been commonly used in many experiments. Here, the irradiated polymer films combined with the untreated FEP film are employed to form TENG devices and the transferred charges from the TENGs have been recorded to illustrate the electrification performance. Moreover, the output currents from the contact electrification between the different polymer films and Al foil have also been measured, as can be seen in Fig. S2 (ESI†).

Meanwhile, different ion irradiation concentrations are applied to the sample, where the ion dose changes from 1×10^{15} to 1×10^{17} ions per cm^2, the results of which can be seen in Fig. 2i–l. The four kinds of polymers are named according to the different ion doses: KAPTON1E15–1E17, PET1E15–1E17, PTFE1E15–1E17, and FEP1E15–1E17. As for the TENG with optimized ion doses, the maximum transferred charge amount of 16.3 nC is achieved with the sample of KAPTON1E16 (1×10^{16} ions per cm^2), where the surface charge density on the KAPTON1E16 film is calculated to be 332 μC m^{-2}. As for the other three cases (irradiated PET, PTFE and FEP), no significant enhancement in the surface charge density has been observed. It is also important to note that with the increase of ion dose, the irradiated PET film can generate more charges than the original PET film, as shown in Fig. 2f. This means that the ion irradiation can increase the electron-donating capability of PET, but this effect is not as significant as that with Kapton. These results confirm that the irradiated Kapton is the main contributor to the enhancement of electrification performance in Fig. 2i, where not only the polarity of Kapton for electrification is switched but also the maximum surface charge density is achieved. Another "negative" polymer film (PVDF) is combined with the four materials after irradiation treatment (ion dose of 1×10^{16} ions per cm^2). The results can be seen in Fig. S3 (ESI†). We further analyze the mechanical and electrical properties of this modified Kapton film, as can be seen in Fig. S4 and S5 (ESI†).

The flexibility of the irradiated Kapton film shows negligible change (Fig. S4, ESI†) and its insulating performance also shows no difference (Fig. S5, ESI†). Since the He irradiation affects the polymer surface, AFM is used to characterize the surface mechanical properties of the Kapton film. The force–indentation data are calculated based on the indentation–deflection results

of the AFM experiment, as can be seen in Fig. S6a and b (ESI†). The amplitudes of the force–indentation changes are almost the same for the Kapton film with and without irradiation. Moreover, the Young's moduli of the samples based on the force data have also been calculated (see the insets of Fig. S6c and d, ESI†). It is found that the scope and trend of the surface Young's modulus of the Kapton film shows almost no difference before and after irradiation.

In order to clarify the underlying mechanism related to the irradiation induced performance change of the Kapton film, in-depth analysis about the morphology and the chemical structure of the Kapton surface has been performed. As can be seen in Fig. S1 (ESI†), after irradiation with He ions with a fluence of 1×10^{16} ions per cm^2, the peak damage level is about 0.26 dpa and the irradiation region depth Rp is about 550 nm with He concentration peak of 0.69%. Cross-sectional samples of the pristine and irradiated materials are studied by using ultrathin sectioning and transmission electron microscope (TEM) measurements. Since Kapton is composed of four elements (C, N, O, and H), EDS and X-ray mappings (Fig. 3a) are used to observe the irradiation area of the cross-sectional sample, and to understand the distribution of each element. On the surface of the irradiated sample, the elements remain uniformly distributed without agglomeration or new phase formation. Fig. 3b shows representations of the top and bottom regions of a sample cross-section of the irradiated sample, while Fig. S7a (ESI†) shows TEM images of the untreated Kapton sample. It can be seen that the injection of the ion beam induces a certain trajectory in the thickness direction of the material and a jagged surface region is observed after ultrathin sectioning. Hence, the ion beam bombards the molecular chain localized in the surface region, causing the chemical bonds and molecular chains to break. Accordingly, after mechanical slicing, the top part of the sample surface has a broken zigzag structure (the jagged region), which is caused by the ion irradiation. The jagged region near the top surface has a depth of 575 nm, which is consistent with the SRIM simulation results in Fig. S1 (ESI†). The dispersive diffraction ring indicates that the irradiation doesn't cause crystallization and the material remains disordered.

On the other hand, through the AFM measurements (Fig. S7b and c, ESI†), we find that ion irradiation can induce a series of tiny collapsing spots on the surfaces of Kapton films. These collapsing spots usually have a diameter of 200 nm and an average depth of 2 nm, which are randomly distributed on the surface of irradiated Kapton. These collapsing spots are due to the generated stress concentration during the impact process of high energy ions. The increase of the roughness usually leads to an increase of effective contact area. However, with the consideration of the detailed value of roughness change, it can only bring a very small change to the electrification process. Therefore, we must consider the changes in the chemical structure, such as some transformations of molecular chains or chemical bonds, in order to explain the irradiation induced changes in both the triboelectric polarity and the charge density.

Polymer materials can have three structural changes during irradiation: degradation, cross-linking, and branching. The structural defects induced by the irradiation can be revealed by
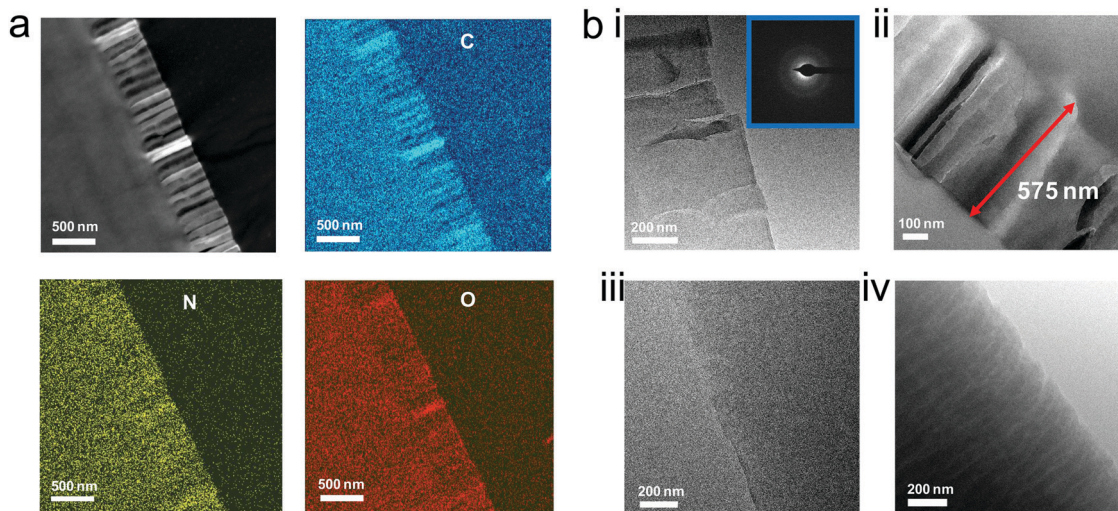
Fig. 3   (a) The HAADF-STEM image and X-ray maps of various elements in the cross-sections of irradiated (KAPTON1E16) samples. (b) The TEM images and diffraction pattern of the cross-sectional region of the irradiated sample (KAPTON1E16): the top part (facing irradiation) (i and ii) and the bottom part (iii and iv) regions.

comparing the microstructure of the sample before and after ion irradiation through TEM observations. It is difficult to describe the structural defects of disordered polymer materials with untight structures, conventional holes, dislocations or void defects. Here, we can use the change in free volume to analyze their irradiation defects.[32] Free volume is known to be the interstitial region of the molecular chain, which is considered as the main structural defect to control the atomic vibration of the polymer. Positron annihilation is known to be a powerful tool to characterize defects in materials.[33] When a monochromatic positron beam penetrates a material, positrons annihilate the surrounding electrons at a depth from the surface and emit γ signals with a small energy offset. Some studies have shown that positron annihilation is also an effective method to detect free volume in polymers.[34,35] By analyzing the Doppler broadening (DB) energy spectrum of γ photons emitted, qualitative results of free volume content in Kapton can be obtained. By adjusting the positron energy, we can obtain the free volume contents at different depths. Positron annihilation DB measurements are performed to detect variations in free volume content in these samples. The S parameter indicates the annihilation between positrons and valence electrons of low momentum measured by positron annihilation DB, so the change in the S parameter can demonstrate the evolution of free volume concentration in the polymer.

The depth profiles of the S-parameters for the pristine and irradiated polymers with different doses are given in Fig. 4a. It can be seen that the S parameter decreases in the surface area and tends to a stable value as the depth increases. In order to investigate the changes in structural defects caused by different doses of irradiation, we define $\Delta S/S$ as:

$$\Delta S/S = \frac{S_{\text{irradiated}} - S_{\text{unirradiated}}}{S_{\text{unirradiated}}} \qquad (2)$$

and the curve of $\Delta S/S$ with depth is given in Fig. 4b. The overall trend of the three irradiation doses is that the S-parameters are

smaller than those of the pristine samples at a few hundred nanometers on the surface and gradually return to equilibrium in the deeper region. The main reason for this trend is that the He ion irradiation depth is about 550 nm, and the structural change is mainly in this region. When the irradiation dose is relatively low, the cross-linking decreases the free volume. Then, the increase of cross-linking constrains the molecular motion and reduces the free volume. As the irradiation dose increases, degradation plays a dominant role. Degradation causes the Kapton molecular chain to break and produce small molecules that inhibit the movement of the segments, resulting in a reduction in free volume size and concentration. The change in free volume indicates that the irradiation causes changes in the chemical bonds and molecular chains of Kapton; therefore the electrification performance also changes.

The structural information of the different films is further revealed by the ATR-FTIR spectra. The difference between the unirradiated Kapton and the irradiated Kapton is shown in Fig. 4c and magnified in Fig. 4d–f. The –CHO stretching/bending at 2850 cm^{-1}, which appears simultaneously with the C=O stretching vibration peak (1780 cm^{-1}), is good proof of aldehyde (Fig. 4d). A distinct new peak observed around 3400 cm^{-1} is related to the breaking of the C–N bond and the formation of a new N–H bond. Hence, for irradiated Kapton, there are new peaks appearing in these two places, which proves that a C–H bond and an N–H bond are formed (Fig. 4f), and in other words, the –NHCOR bond is established (an electron donating group). The electron donating capability of a functional group is determined by the inductive effect and the conjugation effect. The C=O in the –NHCOR bond is an electron withdrawing group, which is a typical induction effect, and the –NHCOR bond is a medium electron donating group. Meanwhile, the conjugation effect occurs when the –NHCOR fragment is bonded to a group containing a π bond (p electron). Accordingly, the electron donating effect of the –NHCOR bond
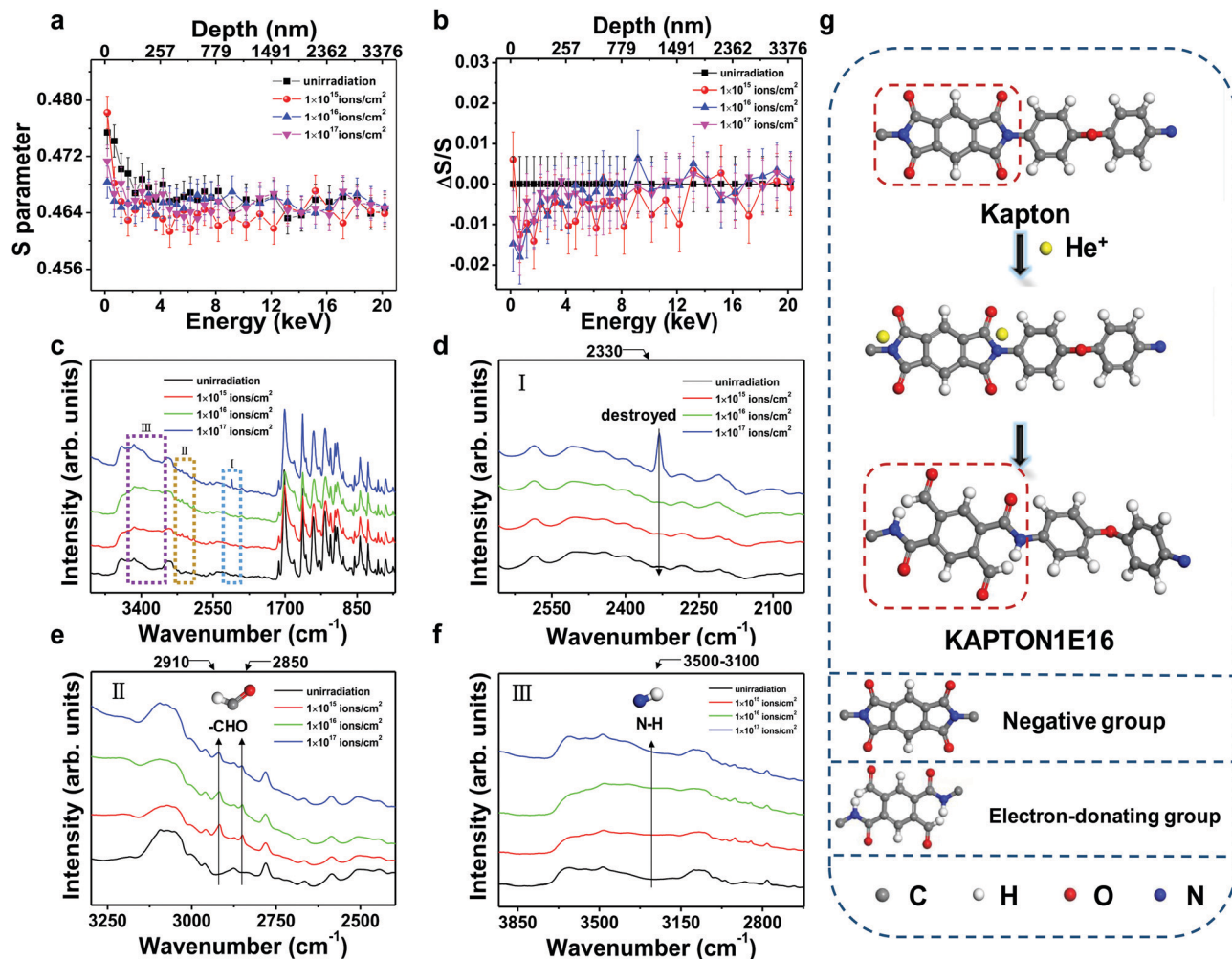
Fig. 4 (a and b) The depth profiles of the S-parameter and the $\Delta S/S$-parameter for the pristine and irradiated polymers with different doses. (c) ATR-FTIR spectra of the Kapton film before and after ion irradiation. (d–f) Corresponding magnified spectra for regions I, II, and III in (c), respectively. The ion dose changes from 1×10^{15} to 1×10^{17} ions per cm^2. (g) Schematic diagram of the molecular formula of Kapton structure change.

is greatly enhanced due to the binding with the benzene ring, which is a kind of conjugation effect (Fig. 4g). The conjugation effect of the –NHCOR bond and the benzene ring leads to the generation of a very strong electron donating group. When KAPTON1E16 is in contact with FEP, more electrons can be supplied due to this conjugation effect. The distinct new peak at 2330 cm^{-1} of the KAPTON1E17 sample suggests that the chemical bond may be destroyed, which leads to the suppression of the charge transfer process (Fig. 4e). In order to confirm that this new peak represents the possible damage of the film, the heavy ion Fe instead of He is selected to irradiate the Kapton film with the same energy and fluence. The measured ATR-FTIR spectrum in Fig. S8a (ESI†) shows that a similar distinct new peak at 2330 cm^{-1} appears when the ion dose of Fe is rather small (1×10^{15} ions per cm^2), indicating that heavy ions can easily damage the film structure at low doses. Meanwhile, due to the irradiation with Fe ions, the C–H peak generated by the Kapton film at 2930 cm^{-1} is the same as that of KAPTON1E16, resulting in the enhancement of the electrification effect (Fig. S8b, ESI†). However, the damage of the film

happens with a low fluence, which decides that the generated surface charge density of Fe-irradiated Kapton is lower than that of KAPTON1E16.

Additionally, in order to study the ultimate product of the Kapton film under high energy irradiation, 400 keV He-radiation is applied to the Kapton film with a fluence of 3×10^{17} ions per cm^2. The SRIM simulation of the irradiation energy is shown in Fig. S9a (ESI†), which is consistent with the dpa of 50 keV at 400 nm. The ATR-FTIR spectrum in Fig. S9b (ESI†) shows that the irradiation with an energy of 400 keV leads to the full carbonization of the film and the transferred charge amount of this carbonized Kapton and FEP can be seen in Fig. S9c (ESI†), which is around 60% of the results from the KAPTON1E16 sample (Fig. 2i). This result proves that low-energy irradiation is suitable for modifying the Kapton film.

So far, we have tried several other ion types with different energies and various fluencies, while an energy of 50 keV, a fluence of 1×10^{16} ions per cm^2 and the He ion are the best irradiation parameters for the Kapton film. In order to further characterize the chemical bonding structures at the molecular

level, we perform the X-ray photoelectron spectroscopy (XPS) measurements for the Kapton and KAPTON1E16 samples. Detailed information on the changes in the chemical structure of the polyimide surface as a result of the ion bombardment is obtained by analyzing the C 1s, O 1s and N 1s peaks in the high resolution XPS spectra. The peak deconvolution of the XPS spectra of the Kapton film has already been thoroughly studied in previous studies.[36] The measured C 1s spectra for the unmodified and modified Kapton in our experiment are shown in Fig. S10a (ESI†). After ion irradiation, the most significant change in the spectra is related to the intensity increase at around 287.5 eV, indicating the formation of a new functional group. This new peak change can be attributed to the breaking of the C–N bond and the formation of aldehyde (–CHO) and amide (–NHCOR) groups due to the He ion irradiation,[37] which can confirm the results from the ATR-FTIR spectra in Fig. 4. As can be seen in the O 1s spectra in Fig. S10b (ESI†), there is no significant change in the peak position of oxygen before and after irradiation, which means that the C=O and C–O bonds are not changed by He ion irradiation. Moreover, as shown in Fig. S10c (ESI†), a single peak corresponding to the C–N imide bond was observed at 400.7 eV in the N 1s spectrum for the untreated Kapton. The peak decreases and shifts to a lower binding energy (399.9 eV) after the ion beam treatment, indicating that the imide ring is broken to form a new functional group. A similar shift of the N 1s peak due to the rearrangement of C–N bonds after nitrogen ion bombardment has also been reported previously.[38] The XPS studies further confirm that He ion irradiation results in chemical structural rearrangements in the Kapton surface, which can support the results from the ATR-FTIR spectra.

In addition, irradiated PET, PTFE, and FEP films are also tested for infrared analysis, as shown in Fig. S11–S13 (ESI†), respectively. The ATR-FTIR spectra of irradiated PET show significant changes in several places and many new peaks can be observed in Fig. S11 (ESI†), which suggests that the PET film has turned into a new polymer. The specific change cannot be further explained only by the ATR-FTIR spectra and we can just briefly identify some characteristic bonds. The irradiated PET generates a new peak (O–H bond) at 3300–3600 cm^{-1}, which shows its electronic donating ability. As the number of incident ions increases, the number of electronic donating groups of the irradiated PET also increases, so the charge transfer amount during the contact electrification increases. PTFE and FEP, which are commonly used as negative electrification materials, have strong electron withdrawing groups because they contain a large amount of F atoms in the molecule. However, the ATR-FTIR spectra of the irradiated PTFE and FEP remain basically unchanged and no corresponding explanation can be given at the molecular structure level. Hence, the He ions with current irradiation energy and fluence may not be enough to change the chemical structures of the PTFE and FEP films. Meanwhile, the irradiation induced surface morphological change has also been studied by using the AFM technique, while no significant change in roughness can be observed on the PTFE and FEP films (Fig. S14, ESI†).

However, there are still some changes in the output performances of these two films after irradiation, as can be seen in Fig. 2. This may due to the charge injection effect caused by ion irradiation. PTFE is a typical electret material, in which the attached free ion and residual electrostatic charge can stay on the surface of PTFE.[39] The experiment in Fig. 2k is the contact between PTFE and FEP, while PTFE is positively charged during the electrification. Hence, it is very likely that the residual electrostatic charges on the PTFE surface are captured by the FEP film during the contact, which further enhances the output performance.

On the other hand, the ion irradiation is performed after vacuum treatment and ion bombardment can also bring the escaping energy to the surface electrostatic charges, which can erase the residual electrostatic charge and the attached free ion on the surface of PTFE.[42] Hence, the induced charge transfer between irradiated PTFE and FEP can be suppressed due to this vacuum treatment. On the other hand, the ion irradiation itself can also bring positive charges to the polymer surface, which can be considered as a kind of charge injection process.[24] During the contact electrification between irradiated PTFE and FEP, these injected He ions can increase the number of positive charges generated on the PTFE surface, which can enhance the electrification process in the same way as in the case of corona polarization or ion implantation by ion gun.[40]

For a lower ion dose (10^{15} ions per cm^2), the injected charges cannot compensate for the charge loss caused by vacuum treatment, and with the increase of ion dose (10^{16} ions per cm^2), the number of transferred charges increases accordingly. In order to verify this effect, we apply vacuum treatment (5×10^{-6} Torr and heating to 60 °C, imitating the conditions of ion irradiation) to the fresh PTFE film without irradiation for about 100 minutes and measured the change in its output performance, as can be seen in Fig. S15a (ESI†). After vacuum treatment, the maximum transferred charge density (σ) of the PTFE film during the contact electrification with the FEP film is significantly decreased. This transferred charge density increases with the increase of motion cycles and finally reaches its saturated value. However, the saturated value of σ is still lower than its original level, as can be seen in Fig. S15b (ESI†). A similar effect can also be used to explain the change in the FEP film. It is also important to note that the charge injection induced by ion irradiation is just a side effect of this irradiation treatment. A Kapton film is a kind of non-electret material, which means that the charge injection effect can only bring negligible influences to the Kapton film.[24] Therefore, in the case of the Kapton film, the induced chemical structure change accounts for the significant performance improvements.

It is noted that a suitable ion, dose and energy need to be properly chosen for a particular polymeric material in order to achieve a desired change in its electrical properties. Currently, the fluence and the energy of this helium ion irradiation are specially designed for modifying the Kapton and PET films, while this parameter cannot effectively modify the chemical structures of the PTFE and FEP films. More importantly, PTFE and FEP have simple molecular structures with only C and F in
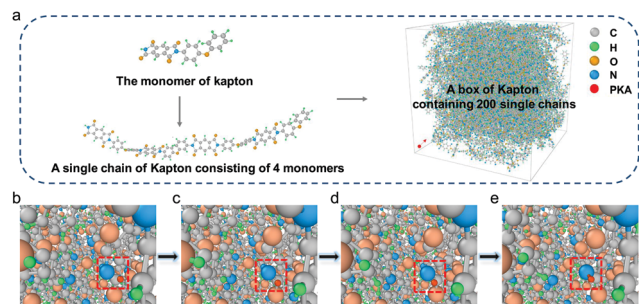
Fig. 5 (a) The model building of the polyimide model irradiation. Atoms are specified by different colors: grey for carbon, green for hydrogen, blue for nitrogen, and yellow for oxygen. The PKA is launched at the red point, heading along the red arrow. (b–e) The breaking and bonding processes of chemical bonds in molecular chains with the molecular dynamics simulation results. And the red ball represents a free hydrogen atom that is disconnected from the molecular chain.

the molecular chain. Even if He ions are able to break their chemical bond, it is still difficult for them to generate a new chemical structure due to the limited chemical elements in the chain. Hence, in order to modify the PTFE or FEP film, we may need to change both the applied energy and the type of irradiated ion. For example, we can try oxygen ions or the combination of both helium and oxygen ions.

The molecular dynamics simulation of Kapton irradiation has been performed, as shown in Fig. 5a. The polyimide model of a Kapton film containing 200 chains with each chain consisting of 4 monomers is fully relaxed in the *NVT* ensemble with dimensions of 72 Å × 72 Å × 72 Å at 300 K. Usually, an injected particle would experience a slow down process and finally rest in a target, making a number of collisions with the target atoms. In these collisions, sufficient energy is transferred from the particle to displace an atom from its original site. The displaced atom is called a PKA (primary knock-on atom)[41] in the field of irradiation. The PKA, which is the atom knocked out from a chain, can in turn displace other atoms, creating a cascade of atomic collisions. Thus, a PKA is created in the left-bottom corner of the box, and launched along the space diagonal direction with a kinetic energy of 1 keV to simulate the collision cascade. The molecular dynamics simulation results, as shown in Fig. 5b–e, indicate that when the charged ions bombard samples, the ions can move longer distances since the Kapton sample itself has many spatial holes. When a certain ion encounters a stable chemical bond, an elastic collision process accompanied by energy transfer can happen. When the kinetic energy obtained by the atoms on these chemical bonds is greater than the breaking bond energy, the corresponding chemical bond is broken and the collision atom is detached by the atoms on these chemical bonds. When the detached atom touches a free atom, a new chemical bond may be formed. In this simulation, the energy transmitted by the collision to the C–N bond is greater than the breaking energy. Hence, the C–N bond begins to break and the N atom leaves the original chemical bond. At the same time, there is also a H atom that breaks away from the chemical bond and becomes a free atom

at a certain speed. In the subsequent process, the N atom and the H atom gradually approach each other and a new N–H bond is formed. Extending into the whole material, the chemical bonds in Kapton's irradiation area continue to break and to be recreated, and eventually many N atoms become free radicals. When combined with H atoms, it leads to the formation of a large amount of amide groups (–NHCOR).

In fact, each molecular chain of the polyimide material has an amide group at both ends, and each repeating unit has a combination of an amide group and an aldehyde group, so ion irradiation destroys their binding and exposes the amide group. In addition to this, there are some amino (–NH) formations. Both the amide group and the amino group are strong electron-donating groups, and when they contact with FEP, they preferentially transmit a large amount of electrons to FEP. Therefore, molecular dynamics visually shows us that the ion radiation passes through the breaking bond and the bonding reaction occurs, which is beneficial to the formation of a large number of positively charged groups to improve the electron-donating capability of the polymer material. The combination of simulation and experimental data clarifies the mechanism about how ion irradiation can change the performance of polymers.

According to the experimental results, we propose a physical picture of the charge transfer mechanism between two dielectric media at room temperature by using the surface state model. In this model, the electrons conform to the Fermi–Dirac distribution function. The work function of dielectric A is lower than that of dielectric B (Fig. 6a), and when the two dielectrics contact with each other (Fig. 6b), the electrons located in the high energy states of dielectric A transfer to the low energy states of dielectric B. After the two dielectrics are separated (Fig. 6c), dielectric A is positively charged, while dielectric B is negatively charged. Then, ion irradiation is applied to dielectric A and the ion injection leads to the generation of more electron-donating groups on the surface of dielectric A, which can finally increase the surface states for electrification (Fig. 6d).
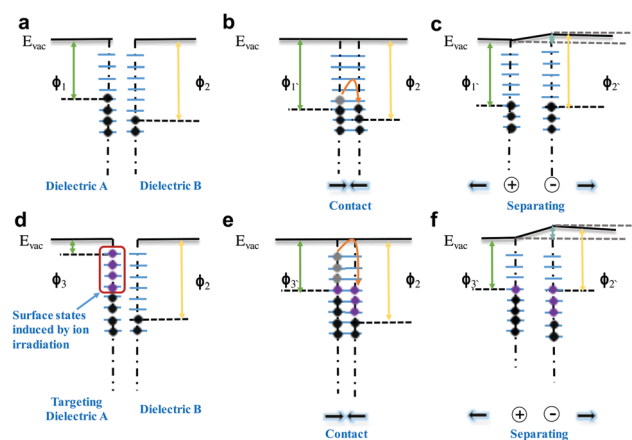
Fig. 6 CE mechanism explained by a surface state model. (a–c) Charge transfer before irradiation of, during contact, and after contact between two different dielectrics, and (d–f) charge transfer after irradiation of, during contact, and after contact between two different dielectrics. ϕ_1 of the unirradiation dielectric is higher than ϕ_3 of the targeting dielectric.
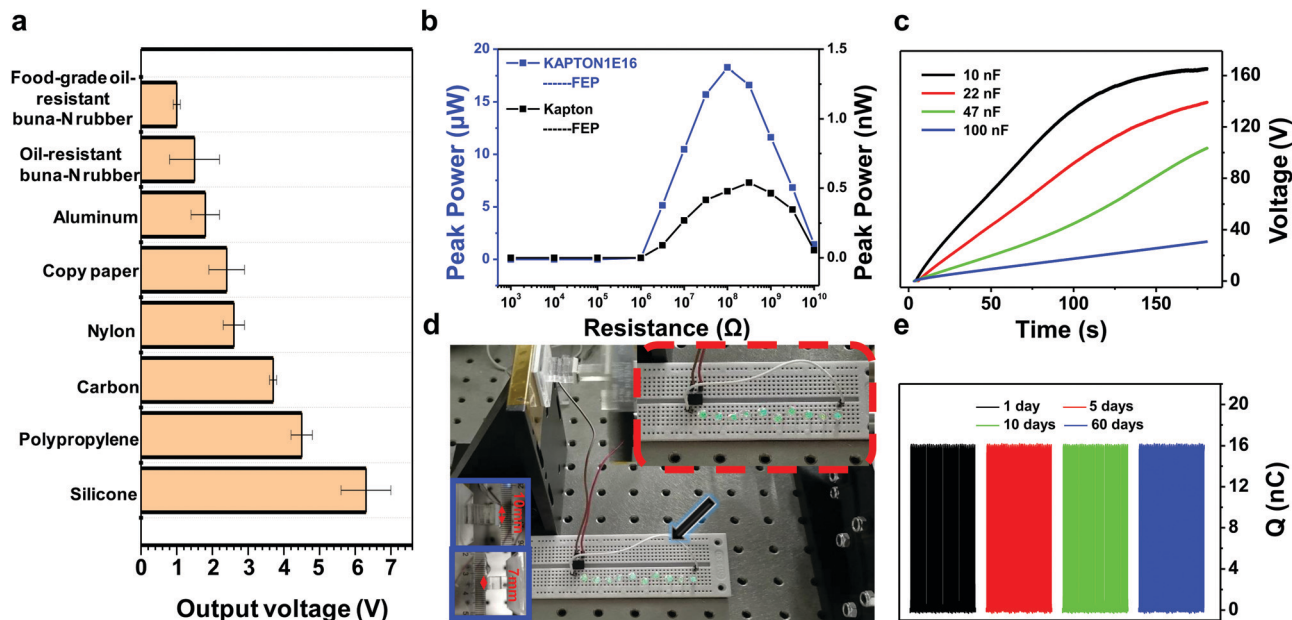
Fig. 7 Different properties of KAPTON1E16: (a) V_{oc} with different positive electrification materials, (b) dependence of peak power on resistance, (c) charging voltage curves for different capacitors with the device in contact with FEP (d) the KAPTON1E16–FEP TENG device with a contact area of 49 mm^2 can light up ten LEDs, and (e) stability of Kapton1E16 in 60 days.

Then, during the contact electrification between dielectric A and dielectric B, more electrons can be transferred onto the interface (Fig. 6e). It is similar to the dielectric-dielectric case in Fig. 6b. After the two dielectrics are separated, targeting dielectric A has more positive charges and the output performance of related TENG devices can be enhanced (Fig. 6f). As can be seen in Fig. 2a and 4g, the strong electron-donating capability induced by ion irradiation on the KAPTON1E16 sample is a very unique and important characteristic. Hence, a further study about its electrification polarity during contact with different materials has been performed, as can be seen in Fig. 7a. Here, eight kinds of materials that usually serve as positive triboelectric materials for TENGs have been selected to work with KAPTON1E16 films. Together, they can form eight different contact–separation type TENG devices with a fixed contact area of 49 mm^2 and the output voltages from these TENG devices with different tribo materials have been recorded, in order to reveal their electrification performance. The results show that the KAPTON1E16 sample has stronger electron-donating capability than all of these materials (Fig. 7a).

It is important to note that the carbonation is an inevitable concern related to Kapton under high energy irradiation. However, the KAPTON1E16 sample can generate a positive output voltage of 3.5 V with pure carbon flakes, which can also rule out the effect of carbonation on the performance change. Meanwhile, it has been reported that food-grade oil-resistant Buna-N/ vinyl rubber is the most positive triboelectric material in the latest triboelectric series,[31] but it still shows weaker electron-donating capability than our KAPTON1E16 sample. Hence, KAPTON1E16 has been chemically modified into an extremely positive triboelectric material, which has the possibility to replace these commonly used positive materials for achieving a TENG device with high outputs.

Of those reported so far, the TENG devices using KAPTON1E16 and FEP films (KAPTON1E16 TENG) as the triboelectric materials exhibit the best performance. Hence, we further analyse the dependence of the peak power on the external resistance for this KAPTON1E16-FEP TENG, as can be seen in Fig. 7b. A reference TENG sample with common Kapton and FEP films is also prepared for the experiment, and the contact areas of both devices are controlled to be 49 mm^2. The maximum peak power of this KAPTON1E16 TENG can reach 18 μW and the maximum peak power of the reference TENG using the common Kapton film is only 0.5 nW. The matching external resistance is around 100 MΩ for both devices. Fig. 7c shows the voltages of different capacitors charged by the combination KAPTON1E16 TENG, where capacitors with capacitances of 100 nF and 47 nF can be charged to voltages of 30 V and 90 V within 200 s, respectively. Furthermore, the KAPTON1E16 TENG with a contact area of 49 mm^2 can light up ten LEDs (Fig. 7d), and we also prepare a video demonstration, as can be seen in the ESI.† The stability of this KAPTON1E16 material is also a key point and the prepared TENG device has been tested for more than 60 days without output degradation (Fig. 7e), which proved that the chemical change in the Kapton film induced by irradiation is quite stable. Hence, the stability of the performance enhancement is also another advantage of this ion irradiation method, especially in comparison with the ion injection method based on corona polarization.

Conclusion

In this work, we have demonstrated a surface modification method for triboelectric materials of TENG devices based on a

high-fluence ion irradiation technique. Four kinds of typical triboelectric polymers, Kapton, PET, PTFE and FEP, have been selected as the targeting materials for He-ion irradiation, and ATR-FTIR spectra combined with morphological scanning measurements have been employed to explain the performance changes of these polymers induced by the ion irradiation. After He-ion irradiation, the electron-donating capability of the KAPTON1E16 sample can be increased to an extremely high level and it can always lose electrons during the contact with almost all the previously reported triboelectric materials, such as Nylon, carbon flakes, and food-grade oil-resistant Buna-N rubber. Accordingly, a contact–separation type TENG has been formed based on KAPTON1E16 and a common FEP film and a surface charge density of up to 332 μC m^{-2} through contact electrification under a normal environment can be achieved, which is higher than those of the previously reported devices using other surface modification methods (ICP etching, ion injection and so on). There are only some methods in external forms, like vacuum protection[42] or charge pumping,[43] that can offer higher charge density. However, they do not rely on the material innovation and the improvements of triboelectric materials can bring fundamental breakthroughs for TENG devices. Both the surface roughness and mechanical performance of the He-irradiated Kapton film show negligible changes, indicating that the change in the chemical structure is the reason for the performance change. The ATR-FTIR spectrum suggests that a strong electron-donating group is generated on the surface of the Kapton film due to the conjugation effect between the benzene ring and the irradiation induced functional group of –NHCOR, which accounts for the significant change in the electrification performance of KAPTON1E16. Moreover, the KAPTON1E16 film can stay for more than 60 days without any protection and no performance degradation can be observed, which proves that the stability is also one of the advantages of this ion irradiation technique. On the other hand, the PET film also generates an electron absorbing group due to irradiation, but the performance change of irradiated PET is not as significant as that of Kapton. Furthermore, there are only very small changes for the PTFE and FEP films in their ATR-FTIR spectra after irradiation, suggesting that the He ions with such irradiation energy and fluence are not sufficient to change their chemical structures. It is important to note that a suitable ion, dose and energy for ion irradiation should be properly selected for a particular polymeric material in order to change certain electrical properties.

Ion irradiation with controllable energy and fluence can directly manipulate the chemical bonds and functional groups of triboelectric polymers at the molecular level, which can help to optimize the detailed performance of TENG devices. Hence, this work not only further enriches the preparation methods of TENGs, but also opens up a new application direction for the traditional ion irradiation technique. Meanwhile, the study of different functional groups and electrification performances also helps us to better understand the electrification process from the viewpoint of chemical structures, suggesting a novel and competitive approach for designing and fabricating TENGs. Based on the current study, we predict that groups like –NR$_2$, –NHR, –NH$_2$, –OH, –OR, –NHCOR, and –OCOR are more likely to lose electrons.

Conversely, groups like –N$^+$R$_3$, –NO$_2$, –CN, and –SO$_3$H tend to absorb electrons with their negative side. Hence, in future studies related to ion irradiation, researchers can pay more attention to the generation of these functional groups, which may create some notable change in the performance of triboelectric polymers. A series of possible future studies in the production of triboelectric materials with different properties can be expected based on the results of this study.

Materials and methods

Materials

The density of polyimide (Kapton) films is 1.40 g cm^{-3}. The density of polyethylene terephthalate (PET) films is 1.37 g cm^{-3}. The density of polytetrafluoroethylene (PTFE) films is 2.2 g cm^{-3}. The density of fluorinated ethylene propylene (FEP) films is 2.15 g cm^{-3}. All the films are commercially available products and used directly without further purification. The pair-wise cutoff radii for bonds can be seen in Table S1 (ESI†).

Irradiation

The polymer samples with dimensions 1 cm × 1 cm are kept as virgin and the others are subjected to irradiation of different doses. Prior to radiation exposure, each polymer film is adhered to the same area of aluminum. The ions are irradiated onto the polymer's surface at room temperature using an NEC 400 kV ion implanter. Most experiments are performed with 50 keV He ions. The applied ion beam potential is 50 kV. The fluence of irradiated ions is changed from 1 × 10^{15} to 1 × 10^{17} ions per cm^2. The projected range value is less than 600 nm for the irradiation experiment calculated by the Monte Carlo based program Stopping and Range of Ions in Matter (SRIM). The details of the irradiation experiments can be found in Table S2 (ESI†).

Molecular dynamics simulation

The Large-scale Atomic/Molecular Massively Parallel Simulator (LAMMPS)[44] is used to study the chemical dynamics of Kapton polyimide bombarded with high-energy particles. The reactive force field (ReaxFF)[45] is implemented to describe the interatomic interactions among C, H, O, and N atoms in Kapton. Besides, a tabulated correction potential based on the Ziegler–Biersack–Littmarck (ZBL) potential[27] has been superposed onto the basic ReaxFF to describe the interatomic interactions in short distances, which is widely used in high-energy collision simulation. The development of this correction potential has been done to be consistent with the LAMMPS implementation of the ReaxFF.[46,47] The collision cascade simulation is performed in a box of 72 Å × 72 Å × 72 Å containing 200 chains. The readers are referred to the ESI† for the details of model building and cascade simulation. The bond energies between atoms can be found in Table S3 (ESI†).

Morphological, electrical and structural characterization

The irradiated polymers are observed with a field-emission scanning electron microscope (SEM, FEI Nova NanoSEM 450).

The pristine and irradiated polymers are fixed with resin and are slice-cut in a frozen environment using a Leica EM UC7 ultra-microtome. The dimensions of the specimens are about 1 mm × 25 μm × 50 nm. Then their microstructures are characterized using a transmission electron microscope (TEM, FEI Tecnai G2 F20). An AFM (MFP-3D from Asylum Research) is used to analyze the surfaces and the effective moduli of the films. The electrical output performance is measured using a Keithley 6514 System Electrometer coupled with a digital linear motor, where the separation distance and the motion frequency of the TENG remain unchanged during all the experiments. The pristine and targeting polymers are scanned from 4000 to 500 cm^{-1} with a Fourier transform infrared (FTIR, VERTEX80v) spectrophotometer in attenuated total reflectance mode (ATR). The X-ray photoelectron spectroscopy (XPS) is performed using a VG ESCALAB MKII spectrometer with an Mg Kα excitation source (1253.6 eV).

Positron annihilation experiment

To characterize structural changes and defects after irradiation of the polymers, the virgin and targeting polymers are analysed using a slow positron beam facility to measure positron annihilation Doppler broadening (DB). The energy range of the positron beam is from 0.18 to 20.18 keV. The relationship between the depth of investigation and incident energy can be expressed by an empirical formula:[48]

$$R = \left(\frac{40}{\rho}\right) E^{1.6}$$

where R is the depth in the materials in units of nm, ρ is the density of polymers in units of g cm^{-3}, and E is the detection energy of the positron beam expressed in keV.

Conflicts of interest

There are no conflicts to declare.

Acknowledgements

References

1 Z. L. Wang, On Maxwell's displacement current for energy and sensors: the origin of nanogenerators, *Mater. Today*, 2017, **20**(2), 74–82.

2 R. D. I. G. Dharmasena, *et al.*, Triboelectric nanogenerators: providing a fundamental framework, *Energy Environ. Sci.*, 2017, **10**, 1039.

3 J. W. Lee, *et al.*, Robust nanogenerators based on graft copolymers via control of dielectrics for remarkable output power enhancement, *Sci. Adv.*, 2017, **3**(5), e1602902.

4 H. Ryu, *et al.*, Sustainable direct current powering triboelectric nanogenerator via intent asymmetrical design, *Energy Environ. Sci.*, 2018, **10**, 1039.

5 C. Dagdeviren, Z. Li and Z. L. Wang, Energy harvesting from the animal/human body for self-powered electronics, *Annu. Rev. Biomed. Eng.*, 2017, **19**, 85–108.

6 H. L. Jeong, *et al.*, Shape memory polymer-based self-healing triboelectric nanogenerator, *Energy Environ. Sci.*, 2015, **8**, 3605–3613.

7 G. Yao, *et al.*, Effective weight control via an implanted self-powered vagus nerve stimulation device, *Nat. Commun.*, 2018, **9**, 5349.

8 C. Dagdeviren, *et al.*, Recent progress in flexible and stretchable piezoelectric devices for mechanical energy harvesting, sensing and actuation, *Extreme Mech. Lett.*, 2016, **9**, 269–281.

9 J. Nie, *et al.*, Power generation from the interaction of a liquid droplet and a liquid membrane, *Nat. Commun.*, 2019, **10**, 2264.

10 J. Nie, X. Chen and Z. L. Wang, Electrically Responsive Materials and Devices Directly Driven by the High Voltage of Triboelectric Nanogenerators, *Adv. Funct. Mater.*, 2018, 1806351.

11 C. Dagdeviren, *et al.*, Flexible piezoelectric devices for gastrointestinal motility sensing, *Nat. Biomed. Eng.*, 2017, **1**(10), 807.

12 B. Zhang, Y. Tang and R. Dai, Breath-based human–machine interaction system using triboelectric nanogenerator, *Nano Energy*, 2019, **64**, 103953.

13 W. Meng, *et al.*, Air-Flow-Driven Triboelectric Nanogenerators for Self-Powered Real-Time Respiratory Monitoring, *ACS Nano*, 2018, **12**, 6156–6162.

14 Z. Saadatnia, E. Esmailzadeh and H. E. Naguib, High Performance Triboelectric Nanogenerator by Hot Embossing on Self-Assembled Micro-Particles, *Adv. Eng. Mater.*, 2018, 1700957.

15 X. Chen, *et al.*, Fluid eddy induced piezo-promoted photodegradation of organic dye pollutants in wastewater on ZnO nanorod arrays/3D Ni foam, *Mater. Today*, 2017, **20**(9), 501–506.

16 B. N. Chandrashekar, B. Deng and A. S. Smitha, Roll-to-Roll Green Transfer of CVD Graphene onto Plastic for a Transparent and Flexible Triboelectric Nanogenerator, *Adv. Mater.*, 2015, **27**(35), 5210–5216.

17 S. Kang, *et al.*, Transparent and conductive nanomembranes with orthogonal silver nanowire arrays for skin-attachable loudspeakers and microphones, *Sci. Adv.*, 2018, **4**, 8772.

18 N. Chuan, T. Lan and Z. Xinya, *et al.*, Washable textile-structured single-electrode triboelectric nanogenerator for

self-powered wearable electronics, *J. Mater. Chem. A*, 2018, **6**, 19143–19150.

19 S. Minsu, *et al.*, Triboelectric Series of 2D Layered Materials, *Adv. Mater.*, 2018, 1801210.

20 S. Park, *et al.*, Capillarity ion concentration polarization as spontaneous desalting mechanism, *Nat. Commun.*, 2016, **7**, 11223.

21 J. Nie, *et al.*, Self-Powered Microfluidic Transport System Based on Triboelectric Nanogenerator and Electrowetting Technique, *ACS Nano*, 2018, **12**, 1491–1499.

22 J. Chun, *et al.*, Mesoporous Pores Impregnated with Au Nanoparticles as Effective Dielectrics for Enhancing Triboelectric Nanogenerator Performance under Harsh Environment, *Energy Environ. Sci.*, 2015, **10**, 1039.

23 E. N. Jayaweera, *et al.*, Triboelectric nanogenerator based on human hair, *ACS Sustainable Chem. Eng.*, 2018, **6**(5), 6321–6327.

24 S. Wang, *et al.*, Maximum Surface Charge Density for Triboelectric Nanogenerators Achieved by Ionized-Air Injection: Methodology and Theoretical Understanding, *Adv. Mater.*, 2014, **26**(39), 6720–6728.

25 Y. X. Liang, *et al.*, High electrocatalytic performance inspired by crystalline/amorphous interface in PtPb nanoplate, *Nanoscale*, 2018, **10**, 11357–11364.

26 C. Sun, *et al.*, Defect engineering of molybdenum disulfide through ion irradiation to boost hydrogen evolution reaction performance, *Nano Res.*, 2019, **12**, 1613–1618.

27 H. Dong and T. Bell, State-of-the-art overview: ion beam surface modification of polymers towards improving tribological properties, *Surf. Coat. Technol.*, 1999, **111**, 29–40.

28 R. Kumar and P. Singh, Influence of SHI upon nanohole free volume and micro scale level surface modifications of polyethyleneterephthalate polymer films, *Appl. Surf. Sci.*, 2015, **337**, 19–26.

29 K. Awasthi, *et al.*, Optical, chemical and structural modification of oxygen irradiated PET, *Radiat. Meas.*, 2010, **45**, 850–855.

30 J. F. Ziegler, M. D. Ziegler and J. P. Biersack, SRIM – the stopping and range of ions in matter, *Nucl. Instrum. Methods Phys. Res., Sect. B*, 2010, **268**, 1818–1823.

31 H. Zou, *et al.*, Quantifying the triboelectric series, *Nat. Commun.*, 2019, **10**, 1427.

32 P. Singh and R. Kumar, Study of structural and free volume properties of swift heavy ion irradiated polyallyl diglycol carbonate polymer films, *Vacuum*, 2013, **96**, 46–51.

33 S. Jin, *et al.*, Correlation between Cu precipitates and irradiation defects in Fe–Cu model alloys investigated by positron annihilation spectroscopy, *Acta Mater.*, 2016, **103**, 658–664.

34 K. M. Flores, *et al.*, Characterization of free volume in a bulk metallic glass using positron annihilation spectroscopy, *J. Mater. Res.*, 2002, **17**(5), 1153–1161.

35 Y. H. Qiu, *et al.*, Mechanisms for the free volume tuning the mechanical properties of metallic glass through ion irradiation, *Intermetallics*, 2018, **101**, 173–178.

36 A. M. Ektessabi and S. Hakamata, XPS study of ion beam modified polyimide films, *Thin Solid Films*, 2000, 621–625.

37 B. D. Silverman, *et al.*, Molecular Orbital Analysis of the XPS Spectra of PMDA-ODA Polymide and Its Polyamic Acid Precursor, *J. Polym. Sci., Part A: Polym. Chem.*, 1986, **24**, 3325.

38 A. Ebe, *et al.*, Improvement of the adhesion to polyimide substrates of copper films prepared by an ion beam and vapor deposition (IVD) method, *Thin Solid Films*, 1996, 356–359.

39 H. Li, *et al.*, Nanocomposite electret with surface potential self-recovery from water dipping for environmentally stable energy harvesting, *Nano Energy*, 2019, **64**, 103913.

40 W. Seung, *et al.*, Boosting Power-Generating Performance of Triboelectric Nanogenerators via Artificial Control of Ferroelectric Polarization and Dielectric Properties, *Adv. Energy Mater.*, 2016, 1600988.

41 M. A. Nastasi, *et al.*, *Ion-solid interactions: fundamentals and applications*, Cambridge University Press, Cambridge, New York, 2004.

42 J. Wang, *et al.*, Achieving ultrahigh triboelectric charge density for efficient energy harvesting, *Nat. Commun.*, 2017, **8**, 88.

43 C. Li, *et al.*, A self-improving triboelectric nanogenerator with improved charge density and increased charge accumulation speed, *Nat. Commun.*, 2018, **9**(1), 3773–3776.

44 S. Plimpton, Fast Parallel Algorithms for Short-Range Molecular Dynamics, *J. Comput. Phys.*, 1995, **117**(1), 1–19.

45 T. P. Senftle, *et al.*, The ReaxFF reactive force-field: development, applications and future directions, *npj Comput. Mater.*, 2016, **2**(1), 15011.

46 H. M. Aktulga, *et al.*, Parallel reactive molecular dynamics: numerical methods and algorithmic techniques, *Parallel Comput.*, 2012, **38**(4–5), 245–259.

47 M. Kanski, *et al.*, Development of a Charge-Implicit ReaxFF Potential for Hydrocarbon Systems, *J. Phys. Chem. Lett.*, 2018, **9**(2), 359–363.

48 P. J. Schultz and K. G. Lynn, Interaction of positron beams with surfaces, thin films, and interfaces, *Rev. Mod. Phys.*, 1988, **60**(3), 701–779.